A Steady-State Equivalent Circuit of TSCAOI Configured Induction Generator for Renewable Energy Conversion Systems

Zhijia WANG and Udaya Kumara MADAWALA

***Abstract*—3-phase cage induction machines, operated in two series-connected and one-isolated (TSCAOI) winding configuration, have been proposed to generate standalone single-phase electricity at variable speeds for renewable energy conversion systems. However, the steady-state behaviour and performance of this particular generator are not yet to be theoretically investigated. This paper therefore presents the first theoretical investigation based on the steady-state equivalent circuit model for standalone TSCAOI configured generators. Moreover, this paper is the first to adopt the winding function approach to derive a dynamic mathematical model for TSCAOI configured generators. This approach not only eliminates the cumbersome mathematical manipulation required in all previous papers related to TSCAOI configured generators but also provides a visual insight into the resulting winding distribution of the machine. In order to investigate the load and excitation characteristics pertinently, the dynamic model is transformed into two different equivalent circuit models by appropriate selected transformation matrix. Using these two models, this paper identified the impacts of system parameters on the load and excitation characteristics, as well as on the level of voltage unbalance. Experimental results of a prototype generator under various operating conditions are presented, together with simulated results, to demonstrate the accuracy of the proposed investigations.**

***Index Terms*—Equivalent circuit model, induction generator, single-phase electricity generation, TSCAOI configuration.**

I. Introduction

DURING the past two decades, clean and sustainable renewable energy resources have drawn wider attentions due to depleting reserves, increasing costs and adverse environmental effects of fossil fuels. Consequently, it has become a common practice within both academia and industry to focus more on renewable energy systems (RESs), emphasising on efficient energy utilization, conversion, transmission, and distribution. The majority of RESs transform kinetic energy into electrical energy, using an electric generator. Different types of generators, such as squirrel cage induction generators (SCIGs), doubly fed induction generator (DFIGs), and synchronous generator (SGs) etc., have been employed in RESs and they differ from one another with respect to operating principles, characteristics, complexity, performance, cost, etc. In particular, SCIG is widely used in RESs due to its low unit cost, ruggedness and virtually free maintenance [1], [2].

Different types of SCIG based RESs have been proposed and implemented over the years, and they can be classified into two groups: (1) fixed-speed SCIG based RESs, and (2) variable-speed SCIG based RESs. In fixed-speed SCIGs, the operating speed may only vary within a narrow band that is up to 1% and the reactive power requirement of SCIGs is normally provided through passive capacitors. The fixed-speed operation of the SCIGs causes a low energy conversion efficiency and the output voltage and frequency depend highly on the load and speed [3], [4], sudden changes of the load and operating speed may even result in collapse of excitation [5], [6]. Therefore, in order to achieve maximum energy conversion efficiency over a wide range of operating speeds and improve the output voltage regulation, the SCIG is normally connected to the utility grid or the loads through a power conversion stage. Such systems are called the variable-speed SCIG based RESs. The main advantages of the variable-speed SCIG based RESs include the improved power quality, increased power output and reduced mechanical stress while the main drawbacks are the increased cost and power losses associated with the power conversion stage.

SCIG has also been employed to generate single-phase electricity, particularly for residential consumption in rural or suburban areas, where both distribution networks and loads are single-phase. Although single-phase SCIMs can be used to supply electricity to single-phase loads, it is more economical and feasible in terms of both cost and size to employ standard 3-phase SCIMs, operated in a single-phase mode, for power ratings above 3 kW [7], [8]. Therefore, use of fixed-speed 3-phase SCIM for single-phase electricity generation has widely been explored, proposing new techniques with successful implementations but with some inherent drawbacks [5]–[9]. To overcome these drawbacks, a number of attempts have been made. For example, power electronic converters were incorporated to improve the voltage and frequency regulation capability of 3-phase SCIM based

Manuscript received December 2, 2019; revised May 28, 2020 and September 30; accepted November 23, 2020. Date of publication March 30, 2021; date of current version March 2, 2021.

Both authors are with the Department of Electrical and Computer Engineering, University of Auckland, Auckland, New Zealand (e-mail: zwan169@aucklanduni.ac.nz; u.madawala@auckland.ac.nz).

Digital Object Identifier 10.24295/CPSSTPEA.2021.00002

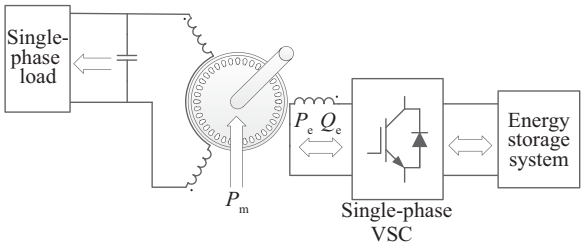

Fig. 1. 3-phase SCIG in TSCAOI configuration.

single-phase electricity generation systems. Use of two full-bridge converters in back-to-back configuration has also been considered [10]–[12]. However, use of two full capacity converters with a bulky filter considerably increases the cost and size as well as the complexity of the system. Single-phase electricity was also generated using a 3-phase SCIM with a combination of 3-phase converters and dump load in [13]–[14], but at the expense of significant power losses in the dumped load and large output voltage drops under heavy load conditions. In [15]–[16], an electronic load controller (ELC) assisted 3-phase SCIM has been proposed for standalone single-phase power generation, and subsequently extended for star connected 3-phase SCIMs in Fukami configuration [17]. Although this scheme provides a relatively low-cost and simple solution for 3-phase SCIM based single-phase power generation system, it is only applicable under constant input power conditions and suffers from low-efficiency and high-harmonic distortion at output.

As an alternative, a new winding configuration that uses one of stator phases of a standard 3-phase SCIM as the excitation winding and the remaining two phases connected in series as power winding has been proposed [18]–[22]. This decoupled winding configuration, named TSCAOI (two-series connected and one isolated) and shown in Fig. 1, generates regulated single-phase electricity at constant frequency under varying rotor speeds [20]–[22]. Variable reactive power for this generator is provided through the excitation winding by a small scale bi-directional converter, which is fed by an energy-storage-system (ESS), while single-phase electricity is generated through the power winding. With storage and retrieval of energy under light and heavy load conditions, respectively, the combination of the ESS and the bi-directional converter allows the generation of constant frequency electricity under variable rotor speed. The integration of photovoltaic (PV) panel in the ESS enables the hybrid renewable energy generation (HREG) [23]–[24] which can significantly improve system reliability and energy utilization.

A detailed theoretical investigation into steady-state characteristics of TSCAOI configured generators is yet to be carried-out. This is primarily because the important load and excitation characteristics of TSCAOI generators cannot be directly obtained through the models that have been proposed in the past. Furthermore, the extent of phase unbalance and its dependency on system parameters have also never been analysed. In order to investigate the load and excitation characteristics pertinently, the paper first transforms the dynamic model of TSCAOI configured generators into two different steady-state equivalent circuit models using symmetrical component method. Using these two models, this paper first identified the impacts of system parameters on the load and excitation characteristics, as well as on the level of voltage unbalance. Moreover, this paper is the first to adopt the winding function approach to derive a dynamic mathematical model for TSCAOI configured generators. In comparison to the previous modelling approach, the winding function approach is simpler and directly offers an explicit description of the resulting winding distribution of the TSCAOI configured machine. It is therefore easy to observe that the TSCAOI configured machines can be equivalent to an unsymmetrical 2-phase SCIM, ignoring the slight differences in the stator resistance and leakage inductance. The accuracy of the proposed unified equivalent circuit as well as the analytical expressions is demonstrated through good agreement between theoretical and experimental results.

II. Dynamic Mathematical Model

To obtain a dynamic model of a 3-phase SCIG in TSCAOI configuration, this paper proposes a winding function approach based modelling method, which is relatively simple and avoids lengthy mathematical manipulations in contrast to the approach presented previously. More importantly, the proposed approach also provides a physical insight into this particular generator concept that may not easily be gained from the previous method. First, consider the stator winding distribution of a conventional 3-phase SCIM and each stator phase winding is assumed to be sinusoidally distributed along the air-gap. The winding function can be treated as spatial distribution of the MMF by a unit current flowing in the winding [25]. Taking the magnetic axis of phase "a" as the reference, the winding function of stator phase windings "a", "b" and "c" can be defined, respectively:

$$N_a(\varphi) = \frac{N_s}{2}\cos(\varphi), \tag{1}$$

$$N_b(\varphi) = \frac{N_s}{2}\cos(\varphi - \frac{2\pi}{3}), \tag{2}$$

$$N_c(\varphi) = \frac{N_s}{2}\cos(\varphi - \frac{4\pi}{3}). \tag{3}$$

Where N_s is the per phase total number of turns, φ is the electrical angle with respect to the magnetic axis of phase "a". Secondly, based on the TSCAOI winding arrangement, one of the three windings is separated as the one-isolated (OI) winding and the remaining two windings, being connected in series, constitute the two-series-connected (TSC) winding. Thus, as shown in Fig. 2, with phase "a" as the OI winding for excitation and phase "b" and "c" in series as the TSC winding for single-phase electricity generation, the winding function of these two sets of windings can be readily obtained.

The winding function of the OI winding, being same as that of the phase "a" winding, is give in (4). The winding function of the TSC winding, which is directly related to its

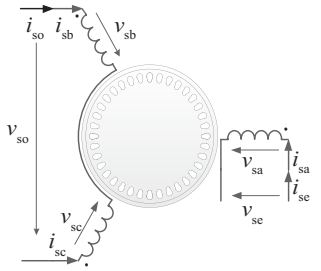

Fig. 2. TSCAOI winding configuration.

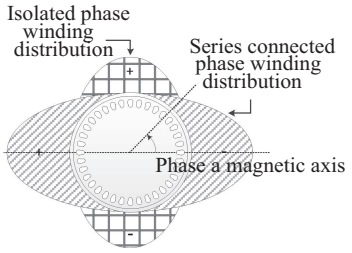

Fig. 3. Effective winding distribution of 3-phase SCIM in TSCAOI configuration.

MMF distribution, is given in (5)

$$N_{se}(\varphi) = \frac{N_s}{2}\cos(\varphi), \tag{4}$$

$$N_{so}(\varphi) = N_b(\varphi) - N_c(\varphi) = \frac{\sqrt{3}\,N_s}{2}\cos\left(\varphi - \frac{\pi}{2}\right). \tag{5}$$

From (4) and (5), it is worthy to note that the TSC winding is still sinusoidally distributed along the air gap but with $\sqrt{3}\,N_s$ turns. Furthermore, both the TSC winding and the OI winding are located with their magnetic axes 90 electrical degrees apart, hence, magnetically decoupled. The effective winding distribution of the 3-phase SCIG in TSCAOI configuration can therefore be represented as in Fig. 3. From Fig. 3, it is easy to observe that the TSCAOI configured 3-phase SCIG can be equivalent to the unsymmetrical two-phase SCIG by ignoring the slight differences in the stator resistance and leakage inductances. Thus, the analytical equations and techniques developed in this paper are also suitable for the power electronic converter based single-phase SCIGs proposed in [26]–[29] as well.

The dynamics of the TSCAOI configured SCIG are modelled in stationary $\alpha\beta$ reference frame. For derivation of the model, it is assumed that the α axis of the $\alpha\beta$ frame is aligned with the magnetic axis of OI winding. Given that the number of turns of the equivalent two phase rotor winding can be arbitrarily selected [30], the 3-phase rotor circuit is referred to a 2-phase rotor circuit with each phase having N_s turns in series. Variables $v'_{r\alpha}$, $v'_{r\beta}$, $i'_{r\alpha}$ and $i'_{r\beta}$ represent the referred α and β components of the rotor voltages and currents. Furthermore, with the series connection of phase "b" and "c" windings, the resistance and leakage inductance of the TSC winding must be twice as much as those of the OI winding. The dependence of voltage equations on the turns ratio between the TSC winding and OI winding can also be eliminated by referring the TSC winding to the OI winding in much the same manner as for rotor circuits. Variables v'_{so} and i'_{so} are the referred voltage and current of the power winding, and v_{se} and i_{se} are the variables of the excitation winding. Consequently, the voltage equations of the stator and rotor circuits in stationary reference frame can be written as:

$$\begin{bmatrix} v_{se} \\ v'_{so} \\ 0 \\ 0 \\ L_m p \\ 0 \\ \frac{2}{3}R_r + \left(\frac{2}{3}L_{lr} + L_m\right)p \\ -\omega_r\left(\frac{2}{3}L_{lr} + L_m\right) \end{bmatrix} = \begin{bmatrix} R_s + (L_{ls} + L_m)p & 0 & L_m p & 0 \\ 0 & \frac{2}{3}R_s + \left(\frac{2}{3}L_{ls} + L_m\right)p & 0 & L_m p \\ L_m p & \omega_r L_m & \frac{2}{3}R_r + \left(\frac{2}{3}L_{lr} + L_m\right)p & \omega_r\left(\frac{2}{3}L_{lr} + L_m\right) \\ -\omega_r L_m & L_m p & -\omega_r\left(\frac{2}{3}L_{lr} + L_m\right) & \frac{2}{3}R_r + \left(\frac{2}{3}L_{lr} + L_m\right)p \end{bmatrix} \begin{bmatrix} i_{se} \\ i'_{so} \\ i'_{r\alpha} \\ i'_{r\beta} \end{bmatrix}. \tag{6}$$

The p represents the operator d/dt, parameters R_s, L_{ls}, L_m, R_r and L_{lr} in (6) represent the stator resistance, the stator leakage inductance, the magnetizing inductance, the rotor resistance and the rotor leakage inductance of the 3-phase induction machine and ω_r is the electrical angular frequency of the rotor in rad/s. The relationship between the referred variables v'_{so} and i'_{so} and actual variables v_{so} and i_{so} can be expressed as:

$$v'_{so} = \frac{v_{so}}{\sqrt{3}} \tag{7}$$

$$i'_{so} = \sqrt{3}\,i_{so}. \tag{8}$$

The electromagnetic torque impressed on the rotor shaft can be expressed as:

$$T_e = \frac{p}{2}L_m(i'_{so}i'_{r\alpha} - i'_{se}i'_{r\beta}). \tag{9}$$

(6)–(9) describe only the electrical behaviour of the TSCAOI machine. The motion of the generator is described by

$$T_e - T_{load} = \frac{2J}{p}\frac{d\omega_r}{dt}, \tag{10}$$

where J is the inertia in kg • m^2, p is the number of poles and T_{load} is the load torque in N_m which includes the torque of the prime mover.

III. Proposed Steady-State Equivalent Circuit

To derive the steady-state unified equivalent circuit model of this particular generator, (6) can be readily translated into steady-state voltage equation via replacing p by $j\omega_s$, where ω_s is the synchronous angular frequency. For unbalanced excitation and load arrangement, the method of symmetrical components,

as proposed in [31], is most commonly used to develop a generalized steady-state equivalent model. Using symmetrical components, the unbalanced phasor variables of the generator can be represented in terms of two sets of balanced phasor variables, each having opposite phase sequence, as given below

$$\begin{bmatrix} \widetilde{X}_{\alpha} \\ \widetilde{X}_{\beta} \end{bmatrix} = [\boldsymbol{S}] \begin{bmatrix} \widetilde{X}_{s+} \\ \widetilde{X}_{s-} \end{bmatrix}. \tag{11}$$

Phasor variables are represented by the tilde symbol (~) over the upper-case variables, and $\widetilde{X}$ in (11) represents any phasor variables of the stator and rotor circuits in the $\alpha\beta$ reference frame, [$\boldsymbol{S}$] is corresponding transformation matrix and the positive sequence and negative sequence symmetrical components are denoted by subscripts s+ and s−, respectively. However, according to the symmetrical components theory, the selection of [$\boldsymbol{S}$] is not unique, and appropriately selected [$\boldsymbol{S}$] will enable the derived equivalent circuit to pertinently investigate either the load or excitation characteristics of the generator, under the steady-state conditions.

A. Equivalent Circuit to Investigate Load Characteristics

In order to derive an equivalent circuit to investigate the load characteristics of the generator, the transformation matrix [$\boldsymbol{S}$] is defined by

$$[\boldsymbol{S}] = \frac{1}{2}\begin{vmatrix} -j & 1 \\ j & 1 \end{vmatrix}. \tag{12}$$

Based on (12), voltage equations in terms of the symmetrical components are obtained by

$$\begin{bmatrix} \widetilde{V}_{s+} \\ \widetilde{V}_{s-} \\ 0 \\ 0 \end{bmatrix} = \begin{bmatrix} \frac{5}{6}R_s + \frac{5}{6}j\omega_s L_{ls} + j\omega_s L_m & -\frac{1}{6}R_s - \frac{1}{6}j\omega_s L_{ls} \\ -\frac{1}{6}R_s - \frac{1}{6}j\omega_s L_{ls} & \frac{5}{6}R_s + \frac{5}{6}j\omega_s L_{ls} + j\omega_s L_m \\ j\omega_s L_m & 0 \\ 0 & j\omega_{syn} L_m \end{bmatrix}$$

$$\begin{bmatrix} j\omega_s L_m & 0 \\ 0 & j\omega_s L_m \\ \frac{1}{s}\frac{2}{3}R_r + j\omega_s\left(\frac{2}{3}L_{lr} + L_m\right) & 0 \\ 0 & \frac{1}{2-s}\frac{2}{3}R_r + j\omega_s\left(\frac{2}{3}L_{lr} + L_m\right) \end{bmatrix} \begin{bmatrix} \tilde{I}_{s+} \\ \tilde{I}_{s-} \\ \tilde{I}_{r+} \\ \tilde{I}_{r-} \end{bmatrix}. \tag{13}$$

where s is the slip. The referred output voltage $\widetilde{V}'_{so}$ is equal to $-Z'\widetilde{I}'_{so}$ and Z' is the referred load impedance, equaling to $Z/3$. According to (12), the symmetrical components of stator voltages can be given as:

$$\widetilde{V}_{s+} = -\frac{j}{2}\widetilde{V}_{se} + \frac{1}{2}\widetilde{V}'_{so} = -\frac{j}{2}\widetilde{V}_{se} - \frac{1}{2}Z'I'_{so} \tag{14}$$

$$\widetilde{V}_{s-} = \frac{j}{2}\widetilde{V}_{se} + \frac{1}{2}\widetilde{V}'_{so} = \frac{j}{2}\widetilde{V}_{se} - \frac{1}{2}Z'I'_{so}, \tag{15}$$

and, $\widetilde{I}'_{so}$ can be further replaced by $(\widetilde{I}_{s+} + \widetilde{I}_{s-})$. Substituting (14) and (15) into (13), (16) is obtained by

$$\begin{bmatrix} -\frac{j}{2}\widetilde{V}_{se} \\ \frac{j}{2}\widetilde{V}_{se} \\ 0 \\ 0 \end{bmatrix} = \begin{bmatrix} \frac{5}{6}R_s + \frac{5}{6}j\omega_s L_{ls} + j\omega_s L_m + \frac{1}{2}Z' & -\frac{1}{6}R_s - \frac{1}{6}j\omega_s L_{ls} + \frac{1}{2}Z' \\ -\frac{1}{6}R_s - \frac{1}{6}j\omega_s L_{ls} + \frac{1}{2}Z' & \frac{5}{6}R_s + \frac{5}{6}j\omega_s L_{ls} + j\omega_s L_m + \frac{1}{2}Z' \\ j\omega_s L_m & 0 \\ 0 & j\omega_s L_m \end{bmatrix}$$

$$\begin{bmatrix} j\omega_s L_m & 0 \\ 0 & j\omega_s L_m \\ \frac{1}{s}\frac{2}{3}R_r + j\omega_s\left(\frac{2}{3}L_{lr} + L_m\right) & 0 \\ 0 & \frac{1}{2-s}\frac{2}{3}R_r + j\omega_s\left(\frac{2}{3}L_{lr} + L_m\right) \end{bmatrix} \begin{bmatrix} \tilde{I}_{s+} \\ \tilde{I}_{s-} \\ \tilde{I}_{r+} \\ \tilde{I}_{r-} \end{bmatrix}. \tag{16}$$

(16) can be represented by the equivalent circuit shown in Fig. 4(a), with explicit relationship to load Z'. The theoretical and experimental results presented in the next section correspond to an operating range of ± 5% synchronous speed, which is reasonable for maintaining the voltage unbalance within acceptable limits. Therefore, the reflected rotor resistance $4R_r/3s$ with the forward field is much larger than the reflected rotor leakage inductance and the corresponding reflected rotor resistance $4R_r/3(2 - s)$ with the backward field is comparable with the rotor leakage inductance. Consequently, as shown in Fig. 4(b), the rotor leakage inductance in the forward field could be ignored and the parallel combination of rotor circuit and magnetizing branch in the backward field could be replaced by the rotor circuit.

Furthermore, in practice, the referred load impedance $Z' >> |-R_s/3 - j\omega_s L_{ls}/3|$. Thus, with above approximations, Fig. 4(a) can be simplified as shown in Fig. 4(b). For clarity, let

$$Z_f \equiv 2j\omega_s L_m \,\|\left(\frac{1}{s}\frac{4}{3}R_r\right) \tag{17}$$

$$Z_1 \equiv 2R_s + 2j\omega_s L_{ls} + j\omega_s \frac{4}{3}L_{lr} + \frac{1}{s-2}\frac{4}{3}R_r. \tag{18}$$

Fig. 4(c) is the simplified version of Fig. 4(b), with new impedances defined above. A simple calculation shows that the voltage across the load impedance is

$$\widetilde{V}'_{load} = \widetilde{V}'_{so} = -Z'\tilde{I}'_{so} = -j\widetilde{V}_{se}\,\frac{Z'(Z_f - Z_1)}{Z'Z_1 + Z'Z_f + Z_1 Z_f}. \tag{19}$$

(19) can now be used to investigate the load characteristics of this generator. The excitation voltage in (19) is obviously a function of load impedance. Regardless of the change of the operating speed, the increased load impedance will reduce the amplitude of the excitation voltage for a specified load voltage. The major drawback of the TSCAOI configured SCIG is its asymmetrical excitation and load arrangement which inevitably cause unbalanced operation of the generator and the associated torque fluctuations. The fluctuating torque,

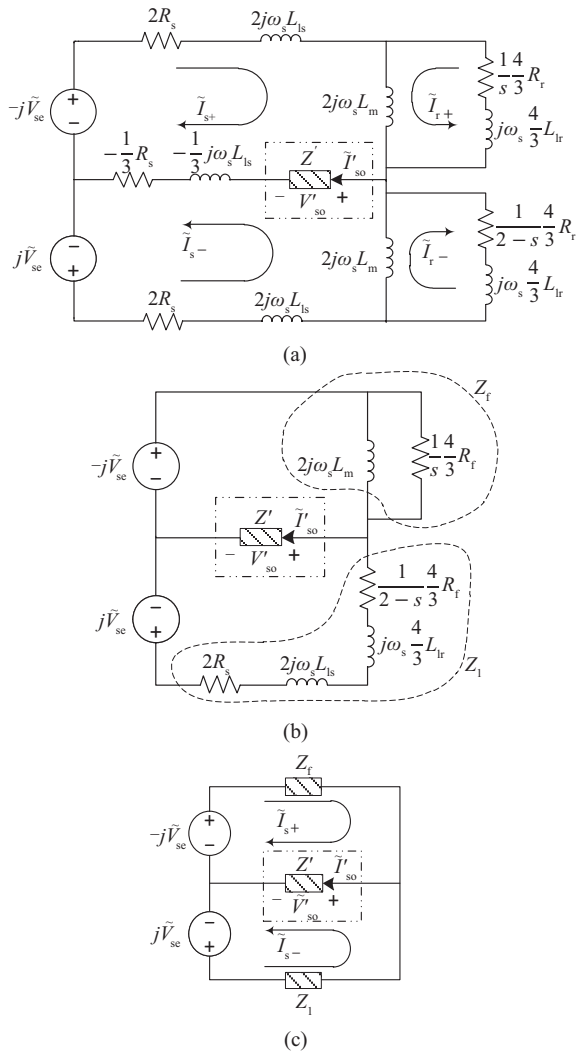

Fig. 4. The unified lumped equivalent circuit to investigate load characteristics (a) Complete equivalent circuit, (b) and (c) simplified circuits.

which is the major source of the audible noise and mechanical vibrations for the unbalanced operating induction generators, not only compromises the overall performance but degrades the operating life of the generator.

However, the difficulties existing in the mathematical manipulation of the electromagnetic torque expression at unbalanced operating condition make it impossible to obtain the detailed approach to reduce the fluctuating torque [32]. Therefore, the voltage unbalance factor (VUF) (defined in (20)), which exhibits approximately proportional relationship with the fluctuating torque in Section IV C, is used to represent the level of the torque fluctuations.

$$VUF = \frac{\text{Modulus of the negative sequence voltage}}{\text{Modulus of the positive sequence voltage}} \quad (20)$$

By substituting (19) into (14) and (15), the positive and negative sequence voltages can be both expressed in terms of $\widetilde{V}'_{\text{load}}$, and VUF defined in (20) can be written as:

$$VUF = \left| \frac{2/Z_{\text{f}} + 1/Z'}{2/Z_{\text{l}} + 1/Z'} \right|. \quad (21)$$

In practical use, the parallel combination of the resistive load R_{load} and a compensation capacitor C_{comp} is often employed to constitute the load impedance. Thus, (21) can be expressed as:

$$VUF = \left| \frac{j\left(\omega_{\text{s}} C'_{\text{comp}} - \frac{1}{\omega_{\text{s}} L_{\text{m}}}\right) + \left(\frac{3S}{2R_{\text{r}}} + \frac{1}{R'_{\text{load}}}\right)}{\frac{2}{Z_{\text{l}}} + \frac{1}{R'_{\text{load}}} + j\omega_{\text{s}} C'_{\text{comp}}} \right|, \quad (22)$$

where, R'_{load} and C'_{comp} are the referred R_{load} and C_{comp} respectively. (22) provides not only a comprehensive view of the unbalanced operation of the generator but also a deep insight of how the parameter variations of the proposed equivalent circuit change the generator operation and fluctuating torque. In the practical scheme, the VUF should be maintained as small as possible to approaching the ideal balanced operating condition and minimizing the fluctuating torque and (22) will serve as the guideline for the parameters selection of such generator systems.

B. Equivalent Circuit to Investigate Excitation Characteristics

Similarly, in order to derive an equivalent circuit to investigate the excitation characteristics of the generator, the transformation matrix [***S***] should be appropriately defined by

$$[\boldsymbol{S}] = \frac{1}{2}\begin{bmatrix} 1 & j \\ 1 & -j \end{bmatrix}. \quad (23)$$

Based on (23), the resulting equivalent circuit model, through which the terminal characteristics of the external excitation circuit can be explicitly evaluated, is shown in Fig. 5(a). Similarly, with appropriate approximations, Fig. 5(a) can be replaced by Fig. 5 (b) and Fig. 5 (b) can be further reduced to its simplest form shown in Fig. 5(c).

In Fig. 5(c), both the load circuit and machine itself are represented as an equivalent impedance Z_{eq} in series with the excitation voltage source. The expression of the excitation current can be readily obtained as:

$$\tilde{I}_{\text{se}} = \frac{\widetilde{V}_{\text{se}}}{Z_{\text{eq}}} = \widetilde{V}_{\text{se}}\left(\frac{3S}{R_{\text{r}}} + \frac{1}{R'_{\text{load}}}\right) + j\widetilde{V}_{\text{se}}\left(-\frac{2}{\omega_{\text{s}} L_{\text{m}}} + \omega_{\text{s}} C'_{\text{comp}}\right). \quad (24)$$

In (24), the first two terms represent the active component of the excitation current and the last two terms represent the reactive component of the excitation current, these two components are of great importance in the study of this particular generator. From (24), it is clear that, for a given excitation voltage, the magnitude of no-load excitation current is always minimum at synchronous speed ($s = 0$) regardless of machine parameters, and when the load is connected, the minimum magnitude of the excitation current is achieved at $s = -R_{\text{r}}/3R'_{\text{load}}$. In (24), it is observed that the reactive component

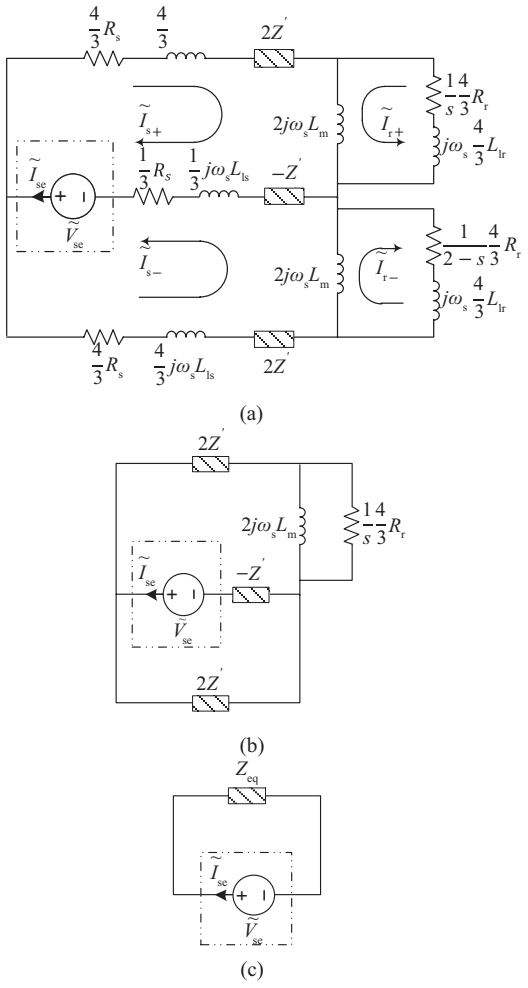

Fig. 5. The unified lumped equivalent circuit to investigate excitation characteristics (a) Complete equivalent circuit, (b) and (c) simplified circuits.

of the excitation current is mainly influenced by both the magnetizing inductance and shunt compensation capacitance. In addition, a properly selected compensation capacitance will significantly reduce the reactive power requirement of the bi-directional converter.

IV. Results and Discussions

In order to demonstrate the practical viability of the standalone TSCAOI configured generator, a prototype generator was configured in the TSCAOI winding arrangement, using a 4-pole, 3 kW, 400 V cage induction machine. The parameters of this cage induction machine are given in the Appendix. A small-scale generation system based on this prototype generator was implemented with the experimental platform shown in Fig. 6.

In the experiment, the prototype generator was mechanically coupled with another induction machine controlled by a variable-speed drive (VSD) for emulating the variable-speed prime mover. A variable resistive load was connected with the power winding, and a single-phase voltage source converter (VSC) was connected with the excitation winding to regulate

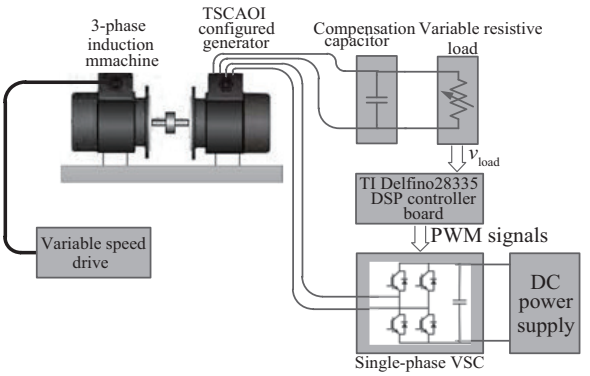

Fig. 6. Experimental setup.

the load voltage at 230 V/50 Hz under varying rotor speeds.

The control software of the single-phase VSC was developed on a TI Delfino 28335 controller board. The load voltage was measured by the isolated voltage sensor, and the feedback signal of the load voltage was read by the control board through A/D (analog to digital) converter. Then, the measured load voltages are converted to a root-mean-square (RMS) value and compared with the 230 V. The voltage error is fed to a proportional-integral (PI) controller. This PI controller regulates the excitation voltage magnitude by providing the reference of the excitation voltage magnitude. The frequency of generation is set by a fixed-frequency (50 Hz) oscillator, the output of which is multiplied with the excitation voltage magnitude reference to produce a sinusoidal excitation voltage reference for the full-bridge converter. Based on the excitation voltage reference, the controller board provides the pulse width modulation (PWM) signals to the VSC.

Before the detailed simulated and experimental investigations, the value of the compensation capacitor must be first determined. The compensation capacitor, connected with the resistive load in parallel, was employed to reduce the reactive-power requirement of the VSC, having a significant impact on the system operating range.

For this particular generation system, its operating range is dependent on both its load range and speed range. Once the operating criteria and compensation capacitor are determined, a specified combination of the load resistance and rotor speed can be justified.

The formulation of the operating criteria mainly considers two aspects, namely the maximum operating current and voltage and the VUF. The detailed operating criteria for this prototype generator are list as following:

- The operating phase currents and voltages are limited within 8.5 A and 300 V respectively.
- Operating the generator with as small torque fluctuation as possible by maintaining the current unbalanced factor (VUF) under 0.15.

The blue shaded region in Fig. 7 indicates the simulated operating range satisfying the above criteria, when the prototype generator was connected with a 20 μF compensation capacitor, supplying power to the resistive load at 230 V/50 Hz. The area of the blue shaded region can be used to quantify the operating range of the generator. Therefore, the

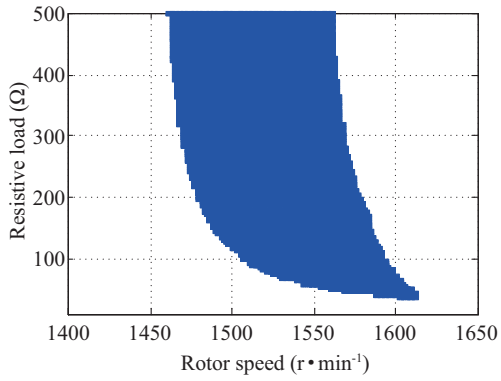

Fig. 7. Operating range of the prototype generator when a 20 μF compensation capacitor was connected.

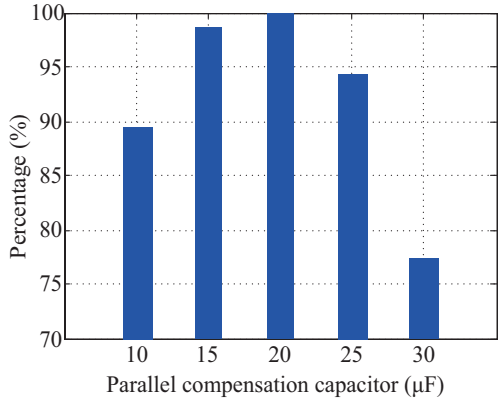

Fig. 8. Operating range comparison using different compensation capacitors.

compensation capacitor can be selected by comparing the areas of the blue shaded regions with respect to different capacitors. Fig. 8 illustrates the comparable quantified operating ranges of this prototype generator using different compensation capacitors. According to Fig. 8, the 20 μF capacitor provides the maximum operating range, was therefore selected.

Fig. 9 shows the contour plots simulated by Matlab for the current variations of the excitation winding and the power winding, respectively, with varying loads and rotor speeds, when the load voltage is regulated at 230 V/50 Hz. At light loads, it is clear from Fig. 9(a) that the minimum excitation winding current is achieved at rotor speeds slightly above the synchronous speed. At heavy loads, however, the speed corresponding to the minimum excitation winding current increases substantially with increasing load. In contrast, the power winding current varies only with the changing loads, as shown in Fig. 9(b), because the load voltage is regulated at 230 V/50 Hz for all speeds.

The contour showing the variations of the excitation winding voltage with the changing loads and rotor speeds are presented in Fig. 10, when the load voltage is regulated at 230 V/50 Hz. As shown in Fig. 10, the required excitation winding voltage should be augmented when the heavier load is connected, over a wide range of rotor speeds.

The detailed simulated and experimental variations of

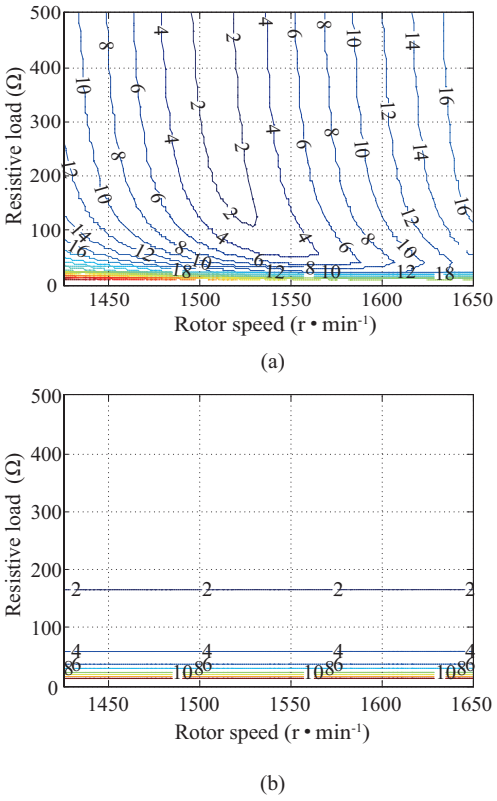

Fig. 9. Variations of the excitation winding current. (a) The power winding current and (b) with the changing loads and rotor speeds.

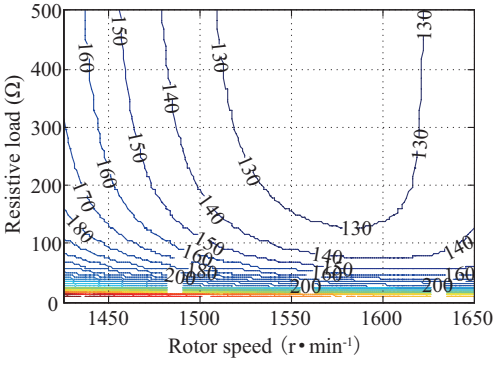

Fig. 10. Variations of the excitation winding voltage with the changing loads and rotor speeds.

the excitation winding voltage versus the rotor speeds are illustrated in Fig. 11, for three different resistive loads. The simulated and experimental results are in agreement and exhibit the same trend. As observed earlier in Fig. 10, Fig. 11 consistently indicates that excitation winding voltage is needed to increase with the increasing of the load, when the output voltage is regulated at a fixed value. Besides, although the impedance seen from the excitation winding is complex in nature, being dependent on both the synchronous angular frequency and the slip frequency, the decrement in the required excitation winding voltage with the increasing of the rotor speed is obvious in Fig. 11.

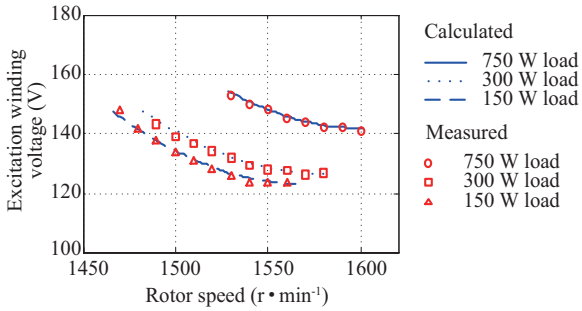

Fig. 11. Variations of the excitation winding voltage with the changing rotor speeds when three different loads are connected.

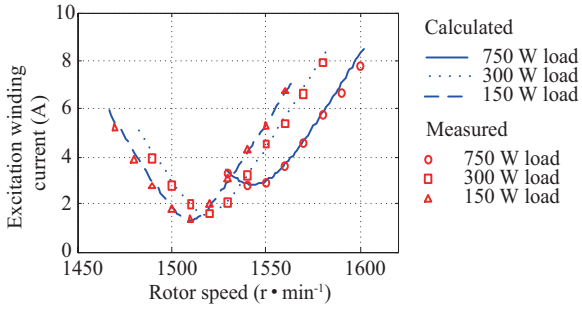

Fig. 12. Variations of the excitation winding current with the changing rotor speeds when three different loads are connected.

Fig. 12 illustrates the variations of the excitation winding current for varying rotor speeds and different resistive loads. It can be noted that, for each load, there exists a unique rotor speed, at which the excitation winding current is minimum.

The variations of the active power provided by the excitation winding for varying rotor speeds and different loads, is illustrated in Fig. 13. The positive power and negative power indicate that the active power is supplied and absorbed by the energy storage system (ESS), connected with the excitation winding, respectively.

It can be noted that, there also exists a unique rotor speed for each load, at which the ESS neither supplies nor absorbs active power. This is because both the load power and losses of the generator, at this speed, are met by the prime mover. In addition, this speed is basically identical to the speed of minimum excitation winding current observed in Fig. 12. Because, when the rotor speed is increased beyond this unique speed, the driven power supplied from the prime mover is increased, and the excess power is therewith absorbed by the ESS, resulting in an increase in the excitation winding current. Similarly, when the rotor speed is reduced below the unique speed, the power of the prime mover is supplemented by the ESS, also resulting in an increase in the excitation winding current.

A. Load Characteristics

The equivalent circuit model, for investigating the load characteristics of the standalone TSCAOI configured generator, has already been obtained in Section III A. Using this model, the relationship between the load voltage and the excitation

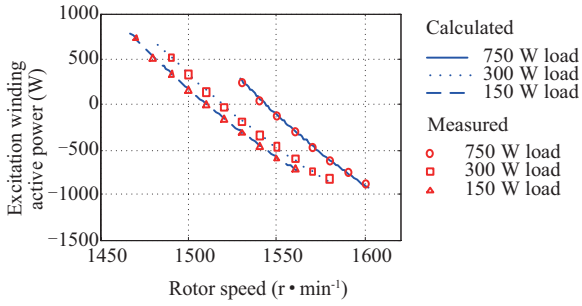

Fig. 13. Variations of the active power of the excitation winding with the changing rotor speeds when three different loads are connected.

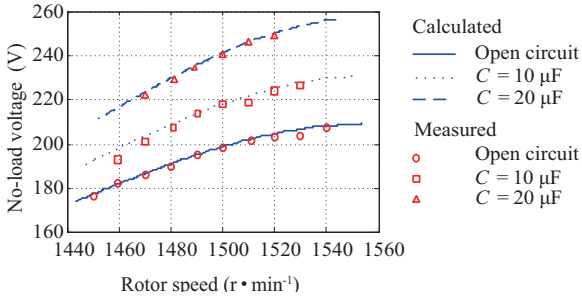

Fig. 14 Variations of the no-load voltage with the changing rotor speeds when three different compensation capacitors are connected and the excitation winding voltage = 135 V/50 Hz.

winding voltage can be explicitly described by (19). According to (19), the load voltage is proportional to the excitation winding voltage, while inverse proportional to the load impedance.

Fig. 14 shows the simulated and experimental variations of the no-load voltage with the changing rotor speeds for three different compensation capacitors, when the excitation winding voltage is fixed at 135 V/50 Hz. It is clearly evident that there exists an inverse relationship between the load voltage and load impedance, when the excitation winding voltage is fixed. Combining with the results shown in Fig. 11, the load characteristics of the standalone TSCAOI configured generator can be comprehensively revealed.

B. Excitation Characteristics

The simulated and experimental variations of the no-load excitation winding currents with the changing rotor speeds for three different compensation capacitors are shown in Fig. 15, when the excitation winding voltage is fixed at 135 V/50 Hz. The good agreements between the simulated and experimental results convincingly indicate that the proposed unified equivalent circuits are accurate and helpful. As could be expected in (24), Fig. 15 shows that the no-load excitation winding current requirement is always minimum at the synchronous speed even though the generator is connected with different compensation capacitors. Furthermore, Fig. 15 indicates that the reactive power requirement of the generator can be effectively compensated by the compensation capacitor, connected to the power winding. From the investigation of the reactive terms

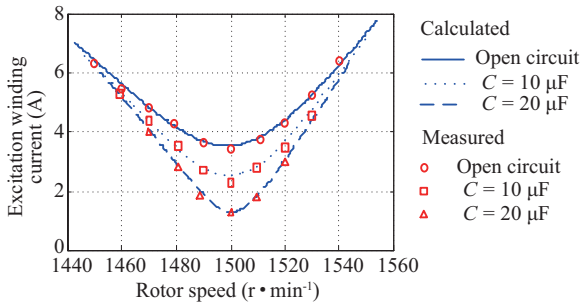

Fig. 15 Variations of the no-load excitation winding current with the changing rotor speeds when three different compensation capacitors are connected and the excitation winding voltage = 135 V/50 Hz.

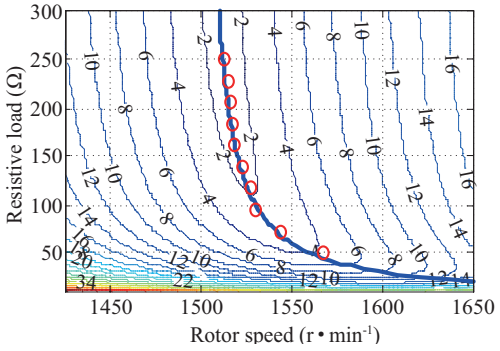

Fig. 16 Contour showing the variations of the excitation winding current with the changing loads and rotor speeds.

in (24), it is notable that the selected compensation capacitor should be as close as to 2/3 $\omega_s^2 L_m$, which is about 31.6 μF, in this case, in order to effectively compensate the reactive power requirement and reduce the excitation winding current.

Fig. 16 shows the simulated variations of the excitation winding current of the generator with varying speeds and different resistive loads, when the load voltage was regulated at 230 V/50 Hz and a 20 μF compensation capacitor is employed. According to (24), the excitation winding current is solely determined by the resistive load and operating speed, with the fixed compensation capacitors. In addition, as explained in Section III B, with a given resistive load, the excitation winding current is always minimum at the operating speed, satisfying $s = -R_r/3R'_{load}$. The thicker blue line, in Fig. 16, denotes the rotor speeds, satisfying $s = -R_r/3R'_{load}$, and the red circles denotes the experimental operating speeds, at which the excitation winding current is minimum with the given resistive load. The good agreements between the theoretical and experimental results further indicate the validity of the analytical equations.

C. Fluctuating Torque and VUF

The major drawback of the TSCAOI configured SCIG is its asymmetrical excitation and load arrangement. This asymmetrical arrangement will inevitably cause unbalanced operation of the generator, which results in torque fluctuations.

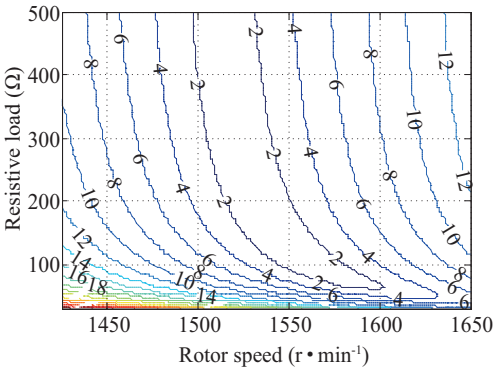

Fig. 17 Variations of the amplitude of the fluctuating torque with the changing loads and rotor speeds when a 20 μF compensation capacitor is connected.

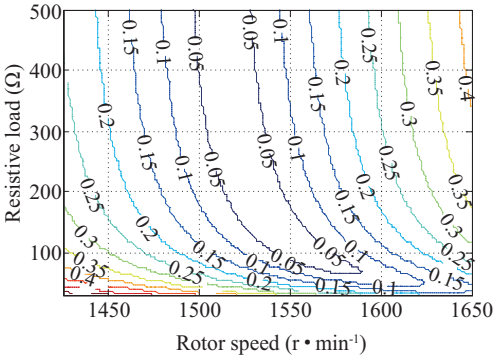

Fig. 18 Variations of VUF with the changing loads and rotor speeds when a 20 μF compensation capacitor is connected.

The fluctuating torque produces audible noise and mechanical vibrations, limiting not only the operating life but also the operating range of generator.

As discussed in [32], the fluctuating torque, which is fluctuating at the frequency of $2\omega_s$, is produced by the stator and rotor currents with opposite phase sequence. This makes the electromagnetic torque of this particular generator very difficult to be mathematically manipulated. However, the V UF and CUF (current unbalance factor) are widely used for evaluating the level of the torque fluctuations, approximately. Fig. 17 shows the simulated variations of the amplitude of the torque fluctuations, with different rotor speeds and resistive loads, while the simulated VUF and CUF variations are shown in Figs. 18 and 19, respectively.

The approximately linear relationship between the amplitude of the torque fluctuation and VUF can be observed from Figs. 17 and 18, the VUF can therefore effectively measure the level of the torque fluctuations, and becomes an important indicator to evaluate the performance of the generator. However, from Fig. 19, it could be found that the CUF is not a good measure to evaluate the level of the torque fluctuations, comparing with the VUF, because, the negative sequence stator current is not always smaller than the positive sequence stator current, which makes the CUF even bigger than 1, especially when the generator is operated at sub-synchronous speeds.

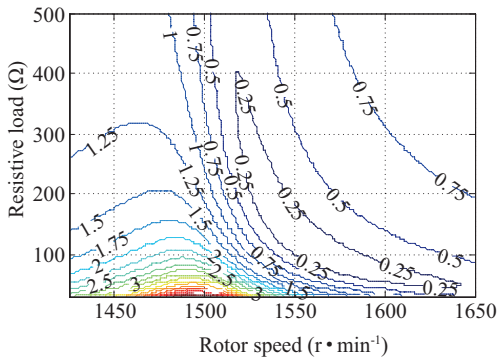

Fig. 19 Variations of CUF with the changing loads and rotor speeds when a 20 μF compensation capacitor is connected.

V. Conclusion

In this paper, two different equivalent circuit models of the TSCAOI configured generator has been proposed to theoretically investigate the excitation and load characteristics of the generator, as well as the impact of machine parameters on performance. A winding function approach based dynamic model has been used to derive the proposed equivalent circuit models and it clearly reveals the equivalent relationship between TSCAOI configured 3-phase SCIG and single-phase SCIG. The techniques presented in this paper can also be applied to study the performance of the previously proposed power electronic converter based single-phase variable-speed SCIG for renewable power generation. Experimental results of a 3 kW SCIM, configured in TSCAOI, has been presented in comparison to theoretical results under various operating conditions to demonstrate the accuracy of the proposed equivalent circuits. According to results, the proposed equivalent circuits, which is unique being the first unified model, is a valuable tool that gives an accurate insight into the complex behaviour of TSCAOI configured SCIGs.

Appendix

Prototype: A squirrel cage 3 kW TECO four-pole 400 V/50 Hz induction machine, which has the following parameters:

$$R_s = 1.5\ \Omega$$
$$R_r = 2\ \Omega$$
$$L_{ls} = 0.011\ \text{H}$$
$$L_{lr} = 0.011\ \text{H}$$
$$L_M = 0.214\ \text{H}$$
$$J = 0.01\ \text{kg} \cdot \text{m}^2$$

References

[1] R. C. Bansal, "Three-phase self-excited induction generators: an overview," in *IEEE Transactions on Energy Conversion*, vol. 20, no. 2, pp. 292–299, Jun. 2005.

[2] B. Wu, Y. Lang, N. Zargari, and S. Kouro, in *Power Conversion and Control of Wind Energy Systems*. Hoboken, NJ, USA: Wiley, 2011.

[3] S. S. Murthy, "A novel self-induced self-regulated single phase induction generator I. Basic system and theory," in *IEEE Transactions on Energy Conversion*, vol. 8, no. 3, pp. 377–382, Sep. 1993.

[4] J. M. Carrasco, L. G. Franquelo, J. T. Bialasiewicz, E. Galvan, R. C. Portillo Guisado, M. A. M. Prats, J. I. Leon, and N. Moreno-Alfonso,"Power-electronic systems for the grid integration of renewable energy sources: A survey," in *IEEE Transactions on Industrial Electronics*, vol. 53, no. 4, pp. 1002–1016, Jun. 2006.

[5] S. S. Murthy, B. Singh, S. Gupta, and B. M. Gulati, "General steady-state analysis of three-phase self-excited induction generator feeding three-phase unbalanced load/single-phase load for stand-alone applications," in *IEE Proceedings—Generation, Transmission and Distribution*, vol. 150, no. 1, pp. 49–55, Jan. 2003.

[6] A. I. Alolah and M. A. Alkanhal, "Excitation requirements of three phase self-excited induction generator under single phase loading with minimum unbalance," *in 2000 IEEE Power Engineering Society Winter Meeting*. Conference Proceedings (Cat. No.00CH37077), Singapore, 2000, pp. 257–259, vol. 1.

[7] T. F. Chan, "Performance analysis of a three-phase induction generator connected to a single-phase power system," in *IEEE Transactions on Energy Conversion*, vol. 13, no. 3, pp. 205–213, Sep. 1998.

[8] S. N. Mahato, S. P. Singh, and M. P. Sharma, "Capacitors required for maximum power of a self-excited single-phase induction generator using a three-phase machine," in *IEEE Transactions on Energy Conversion*, vol. 23, no. 2, pp. 372–381, Jun. 2008.

[9] A. H. Al-Bahrani and N. H. Malik, "Steady state analysis and performance characteristics of a three-phase induction generator self excited with a single capacitor," in *IEEE Transactions on Energy Conversion*, vol. 5, no. 4, pp. 725–732, Dec. 1990.

[10] R. Bojoi, D. Roiu, G. Griva, and A. Tenconi, "Single-phase grid-connected distributed generation system with maximum power tracking," in *2010 12th International Conference on Optimization of Electrical and Electronic Equipment*, Basov, 2010, pp. 1131–1137.

[11] B. K. Bose, "Energy, environment, and advances in power electronics," in *IEEE Transactions on Power Electronics*, vol. 15, no. 4, pp. 688–701, Jul. 2000.

[12] M. G. Simoes, B. K. Bose, and R. J. Spiegel, "Design and performance evaluation of a fuzzy-logic-based variable-speed wind generation system," in *IEEE Transactions on Industry Applications*, vol. 33, no. 4, pp. 956–965, Jul.-Aug. 1997.

[13] C. P. Ion and C. Marinescu, "Stand-alone micro-hydro power plant with induction generator supplying single phase loads," in *Journal of Renewable and Sustainable Energy*, vol. 5, no. 1, 2013.

[14] C. P. Ion, I. Serban, and C. Marinescu, "Single-phase operation of an autonomous three-phase induction generator using a VSI-DL control system," in *2008 11th International Conference on Optimization of Electrical and Electronic Equipment*, Brasov, 2008, pp. 333–338.

[15] S. S. Murthy, Ramrathnam, M. S. L. Gayathri, K. Naidu, and U. Siva, "A novel digital controls technique of electronic load controller for SEIG based micro hydel power generation," in *2006 International Conference on Power Electronic*, Drives and Energy Systems, New Delhi, 2006, pp. 1-5.

[16] B. Singh, S. S. Murthy, and S. Gupta, "Analysis and design of electronic load controller for self-excited induction generators," in *IEEE Transactions on Energy Conversion, vol*. 21, no. 1, pp. 285–293, Mar. 2006.

[17] S .Gao, G. Bhuvaneswari, S. S. Murthy, and U. Kalla, "Efficient voltage regulation scheme for three-phase self-excited induction generator feeding single-phase load in remote locations," in *IET Renewable Power Generation*, vol. 8, no. 2, pp. 100–108, 2014.

[18] A. Chatterjee and D. Chatterjee, "An improved excitation control technique of three-phase induction machine operating as dual winding generator for micro-wind domestic application," in *Energy Conversion and Management*, vol. 98, pp. 98–106, Jul. 2015.

[19] A. Chatterjee and D. Chatterjee, "Analysis and control of photovoltaic-assisted three-phase induction machine operating as single-phase micro-wind generator," in *IET Generation, Transmission & Distribution*, vol. 10, no. 9, pp. 2165–2176, 2016.

[20] U. K. Madawala, T. Geyer, J. B. Bradshaw, and D. M. Vilathgamuwa, "Modeling and analysis of a novel variable-speed cage induction generator," in *IEEE Transactions on Industrial Electronics*, vol. 59, no. 2, pp. 1020–1028, Feb. 2012.

[21] J. Soltani and N. R. Abjadi, "A novel stand-alone single-phase induction generator using a three-phase machine and a single-phase PWM inverter," in *International Journal of Engineering-Transactions A: Basics*, vol. 16, no. 3, pp. 259–268, Sep. 2003.

[22] Z. Wang, U. K. Madawala, T. Liu, and D. J. Thrimawithana, "Steady-state characteristis of 3-phase cage induction generators in TSCAOI configuration," in *2015 IEEE 2nd International Future Energy Electronics Conference (IFEEC)*, Taipei, 2015, pp. 1–6.

[23] M. H. Nehrir, C. Wang, K. Strunz, H. Aki, R. Ramakumar, J. Bing, Z. Miao, and Z. Salameh, " A review of hybrid renewable/alternative energy systems for electric power generation: configurations, control, and applications," in *IEEE Transactions on Sustainable Energy*, vol. 2, no. 4, pp. 392–403, Oct. 2011.

[24] S. Sarkar and V. Ajjarapu, "MW resource assessment model for a hybrid energy conversion system with wind and solar resources," in *IEEE Transactions on Sustainable Energy*, vol. 2, no. 4, pp. 383–391, Oct. 2011.

[25] N. L. Schmitz and D. W. Novotny, inIntroductory Electromechanics. New York, NY, USA: Ronald Press, 1965.

[26] O. Ojo, O. Omozusi, A. Ginart, and B. Gonoh, "The operation of a stand-alone, single-phase induction generator using a single-phase, pulse-width modulated inverter with a battery supply," in *IEEE Transactions on Energy Conversion*, vol. 14, no. 3, pp. 526–531, Sep. 1999.

[27] O. Ojo, O. Omozusi, and A. A. Jimoh, "The operation of an inverter-assisted single-phase induction generator," in *IEEE Transactions on Industrial Electronics*, vol. 47, no. 3, pp. 632–640, Jun. 2000.

[28] M. Myers, M. Bodson, and F. Khan, "Design of drives for inverter-assisted induction generators," in *IEEE Transactions on Industry Applications*, vol. 48, no. 6, pp. 2147–2156, Nov.-Dec. 2012.

[29] O. Ojo and B. Gonoh, "A controlled stand-alone single-phase induction generator," in *Proceedings of International Conference on Power Electronics*, Drives and Energy Systems for Industrial Growth, New Delhi, India, 1996, pp. 694–699, vol. 2.

[30] A. E. Fitzgerald, C. Kingsley, and S. D. Umans, in *Electric Machinery*, 6th ed. New York, NY, USA: McGraw-Hill, 2003.

[31] C. L. Fortescue, "Method of symmetrical co-ordinates applied to the solution of polyphase networks," in *Transactions of the American Institute of Electrical Engineers*, vol. XXXVII, no. 2, pp. 1027–1140, Jul. 1918.

[32] Z. Wang, U. K. Madawala, T. Liu, D. M. Vilathgamuwa, and D. J. Thrimawithana, "Torque characteristics of TSCAOI configured induction generators," in *2016 IEEE 2nd Annual Southern Power Electronics Conference (SPEC)*, Auckland, 2016, pp. 1–6.

Zhijia Wang received the B.E. degree in electrical engineering and automation from the Harbin Institute of Technology, Harbin, China, in 2010, and the M.Sc. degree in automotive engineering from Bath University, Bath, U.K., in 2012. He is currently pursuing the Ph.D. degree with the Department of Electrical and Computer Engineering, the University of Auckland, Auckland, New Zealand. His current research interests include power electronics, electric machine drive and design, and electric vehicles.

Udaya Kumara Madawala graduated with B. Sc. degree (electrical engineering) (Hons) from The University of Moratuwa, SriLanka in 1986 and received his Ph.D. degree (power electronics) from The University of Auckland, New Zealand in 1993 as a commonwealth Doctoral Scholar. At the completion of his Ph.D., he was employed by Fisher & Paykel Ltd., New Zealand, as a Research and Development Engineer to develop new technologies for motor drives. In 1997 he joined the Department of Electrical and Computer Engineering at The University of Auckland where he is a Full Professor at present. His research interests are in the fields of wireless power transfer (WPT), power electronics, V2G applications and renewable energy. Udaya is a Fellow of the IEEE and a Distinguished Lecturer of the IEEE Power Electronic Society (PELS), and has over 30 years of both industry and research experience in the fields of power electronics and energy. He has served both the IEEE Power Electronics and Industrial Electronics Societies in numerous roles, relating to editorial, advisory, conference, technical committee and chapter activities.